

TIME-VARIABLE ALUMINUM ABSORPTION IN THE POLAR AR URSAE MAJORIS, AND AN UPDATED ESTIMATE FOR THE MASS OF THE WHITE DWARF

YU BAI¹, STEPHEN JUSTHAM^{2,1} JIFENG LIU^{1,2}, JINCHENG GUO^{1,2}, QING GAO^{1,2}, HANG GONG^{1,2},

Draft version January 4, 2018

ABSTRACT

We present spectra of the extreme polar AR Ursae Majoris (AR UMa) which display a clear Al I absorption doublet, alongside spectra taken less than a year earlier in which that feature is not present. Re-examination of earlier SDSS spectra indicates that the Al I absorption doublet was also present ≈ 8 years before our first non-detection. We conclude that this absorbing material is unlikely to be on the surface of either the white dwarf (WD) or the donor star. We suggest that this Al I absorption feature arises in circumstellar material, perhaps produced by the evaporation of asteroids as they approach the hot WD. The presence of any remaining reservoir of rocky material in AR UMa might help to constrain the prior evolution of this unusual binary system. We also apply spectral decomposition to find the stellar parameters of the M dwarf companion, and attempt to dynamically measure the mass of the WD in AR UMa by considering both the radial velocity curves of the H_β emission line and the Na I absorption line. Thereby we infer a mass range for the WD in AR UMa of $0.91 M_\odot < M_{WD} < 1.24 M_\odot$.

Subject headings: binaries: spectroscopic — stars: individual (AR Ursae Majoris) — novae, cataclysmic variables

1. INTRODUCTION

The polar AR UMa is inferred to contain a white dwarf (WD) that possesses a magnetic field of ~ 240 MG – the strongest of the known polars (Schmidt et al. 1996; Gänsicke et al. 2001). Its optical observations show that it often changes between high and low brightness states, remaining in the low state for approximately 90% of the time. During the low state, ellipsoidal variations reveal an orbital period of 1.932 hr (Remillard et al. 1994), and both the WD and the M dwarf (MD) donor star can be detected from optical spectra.

Here we report the detection of a time-variable aluminum absorption line in spectra of AR UMa. We conclude that the line probably originates from circumstellar material around the WD, and tentatively suggest that the most likely origin of this material is from evaporation of infalling asteroids.

Similar scenarios have been examined in recent years, with both observational evidence and theoretical studies finding that tidal disruption and evaporation of rocky asteroids can account for circumstellar material around WDs (Lallement et al. 2011; Debes et al. 2012a; Perez-Becker & Chiang 2013; Veras et al. 2014, 2015; Vanderburg et al. 2015). This suggests that reservoirs of asteroids, comets, and planets/planetisimals may exist in wide orbits around some WDs. If so, their orbits could occasionally become sufficiently unstable or elliptical that they are disrupted as they approach the WD (Frewen & Hansen 2014; Stone et al. 2015; Veras et al. 2015). Rocky debris may also be evaporated by the hot radiation from a WD into circumstellar gas, from which heavy element absorption

lines can originate (Lallement et al. 2011; Debes et al. 2012a; Dickinson et al. 2012; Perez-Becker & Chiang 2013). Such scenarios may also explain the features of non-degenerate stars – notably β Pictoris, a star with a well-established debris disk (see, e.g., Beust et al. 1990, 1996; Karmann et al. 2003). Material from an evaporating rocky planet may explain photometric variations in Kepler observations of the K dwarf KIC 12557548 (Rappaport et al. 2012).

Our detection was serendipitous. Despite being a very well-known and extreme system, the basic parameters of the stellar components in AR UMa are poorly constrained. The emission lines from the heated inner hemisphere of the MD are a poor tracer of the barycenter of the MD, and thus have not enabled precise dynamical mass measurements. Using the H_α emission line, Schmidt et al. (1999) estimated the mass of the WD as $0.4 \leq M_{WD} \leq 1.0 M_\odot$. This observing campaign was initially intended to measure the system parameters by taking advantage of the absorption lines from the MD, such as Na I, which are more isotropically distributed over the photosphere of the MD (Rebassa-Mansergas et al. 2007).

Our observations of AR UMa and our updated orbital ephemeris are briefly described in Section 2, the detection of aluminum absorption lines is presented in Section 3, and our new constraints on the system masses and geometry are given in Section 4. Section 5 features potential explanations for the origin of the aluminum absorption lines. A summary is given in Section 6.

2. OBSERVATIONS & BASIC ORBITAL PARAMETERS

Optical spectra of AR UMa were obtained with the Double Spectrograph (DBSP) at the Palomar Observatory. The dichroic D55, which splits light into blue and red channels around 5500 Å, was used with two 1200 line mm^{-1} gratings blazed at 5000 and 9400 Å, respectively.

¹ Key Laboratory of Optical Astronomy, National Astronomical Observatories, Chinese Academy of Sciences, 20A Datun Road, Chaoyang District, 100012 Beijing, China; ybai@nao.cas.cn

² College of Astronomy and Space Sciences, University of the Chinese Academy of Sciences, Beijing, China 100049

Table 1
Log of Observations

UT Date (yyyyymmdd)	Number of Exposures		Exposure Time		Wavelength Coverage ($\lambda\lambda$)		Spectral Resolution ($\Delta\lambda$)	
	Blue	Red	Blue (s)	Red (s)	Blue (\AA)	Red (\AA)	Blue (\AA)	Red (\AA)
20120322	4	2	300	600	3990–5540	5680–9010	1.4	2.8
20120518	2	2	600	600	3710–5260	5660–8900	1.4	2.8
20130312	10	10	600	600	3800–5350	8390–9040 ^a	1.4	1.4

^a Unfortunately the CCD in the red side of DBSP was broken; these observations used the smaller backup CCD.

Table 2
Line-fitting Results

HJD–2456000 ^a (day)	Al		H β		NaI	
	Velocity (km s^{-1})	FWHM (\AA)	Velocity (km s^{-1})	FWHM (\AA)	Velocity (km s^{-1})	FWHM (\AA)
–2938.561	22.1 ± 25.2	$1.5 \pm 1.2, 2.6 \pm 1.7$				
8.662	No spectral coverage		231.0 ± 6.5	3.6 ± 0.3	280.1 ± 24.8	$6.9 \pm 1.6, 12.7 \pm 2.8$
8.666	No spectral coverage		175.0 ± 4.0	3.3 ± 0.2		
8.670	No spectral coverage		108.7 ± 2.8	3.2 ± 0.1	189.9 ± 19.0	$16.1 \pm 4.9, 7.0 \pm 1.2$
8.674	No spectral coverage		40.7 ± 2.5	3.0 ± 0.1		
65.752		$< 1.4^b$	-24.4 ± 4.1	3.6 ± 0.2	-105.5 ± 27.8	$7.1 \pm 1.7, 17.9 \pm 4.5$
65.759		$< 1.1^b$	-162.3 ± 4.8	3.3 ± 0.2	-249.5 ± 18.9	$5.5 \pm 1.4, 21.6 \pm 5.9$
363.650	70.2 ± 21.9	$3.8 \pm 1.3, 4.9 \pm 1.2$	200.4 ± 25.9	5.7 ± 1.1	No spectral coverage	
363.683	77.4 ± 18.7	$2.8 \pm 0.9, 4.6 \pm 1.2$	-6.2 ± 4.2	4.0 ± 0.2	No spectral coverage	
363.721	63.4 ± 11.3	$4.0 \pm 0.7, 3.6 \pm 1.6$	67.7 ± 37.4	8.6 ± 1.6	No spectral coverage	
363.761	42.5 ± 27.5	$4.8 \pm 1.4, 5.1 \pm 2.0$	45.7 ± 3.9	3.9 ± 0.2	No spectral coverage	
363.799	44.9 ± 14.8	$3.9 \pm 0.8, 4.6 \pm 0.9$	-17.1 ± 20.1	3.8 ± 0.8	No spectral coverage	
363.837	48.8 ± 17.0	$3.8 \pm 1.3, 3.8 \pm 0.8$	119.1 ± 2.8	4.1 ± 0.1	No spectral coverage	
363.875	49.4 ± 13.1	$3.3 \pm 0.7, 4.9 \pm 0.8$	-72.9 ± 17.9	4.5 ± 0.7	No spectral coverage	
363.913	59.8 ± 14.1	$2.8 \pm 0.7, 3.5 \pm 0.8$	200.9 ± 4.6	3.8 ± 0.2	No spectral coverage	
363.950	65.5 ± 16.3	$3.0 \pm 0.8, 3.8 \pm 1.0$	-168.7 ± 17.3	5.2 ± 0.7	No spectral coverage	
363.976	77.4 ± 12.5	$4.2 \pm 0.8, 3.2 \pm 0.6$	234.7 ± 10.1	4.1 ± 0.4	No spectral coverage	

^a Heliocentric Julian date.

^b For the strongest individual line from the doublet.

Table 3
Fitting parameters of radial velocities

Line	K (km s^{-1})	γ (km s^{-1})	P (hr)
Al	17 ± 9	61 ± 6	8.891 ± 0.001
H β	248 ± 4	34 ± 5	1.93201522^a
Ca II	275 ± 15	30 ± 7	1.93201522^a
NaI	409 ± 26	34^b	1.93201522^a

^a Given by the updated ephemeris.

^b Fixed to the γ of H β .

After each exposure of AR UMa, two exposures each of FeAr (blue channel) and HeArNe (red channel) lamps were taken to minimize the systemic uncertainty in the wavelength calibration. The standard stars Hiltner 600 and Hz 44 were observed before and after the exposures of AR UMa. All observations are summarized in Table 1.

The spectra were reduced in a standard way using IRAF procedures. After bias subtraction and flat correction, the one-dimensional (1D) spectra were extracted with an aperture size of 10 pixels. The wavelength calibration of each exposure was carried out using the adjacent arc lamp exposures. Those 1D spectra were then corrected for atmospheric extinction, and flux-calibrated using the exposures of the standard stars.

2.1. Updated Orbital Ephemeris

The H β emission line is the strongest feature in all of our 16 observations. After barycenter correction, we used a Gaussian function plus a parabola (Rebassa-Mansergas et al. 2007) to fit the H β emission line and find its radial velocity (and error) in each observation. These values are presented in Table 2. Assuming a circular orbit (Howell et al. 2001), we then fitted a sine curve to the radial velocities, keeping the period fixed to 0.08050074(12) day (Schmidt et al. 1999) and iteratively minimizing χ^2 . The best solution has a radial velocity amplitude of $K = 245 \pm 4 \text{ km s}^{-1}$ and a systemic velocity of $\gamma = 36 \pm 5 \text{ km s}^{-1}$ (quoting 90% uncertainties).

From this best-fit curve, we took five instances of positive zero-crossing of the radial velocity curve, HJD (2456000 +) 363.641, 363.721, 363.802, 363.882, 363.963 with an uncertainty of 0.008 days. Combining this with the seven instances of positive zero-crossing in Schmidt et al. (1999), we derive a best-fit orbital ephemeris of

$$\text{HJD} = 2450470.4314(4) + 0.080500634(8)E. \quad (1)$$

Fitting our H β emission line radial velocities again using this updated orbital period finds $K = 248 \pm 4 \text{ km s}^{-1}$ and $\gamma = 34 \pm 5 \text{ km s}^{-1}$ (see Table 3). We also fitted the Ca II triplet with the same procedure as H β ,

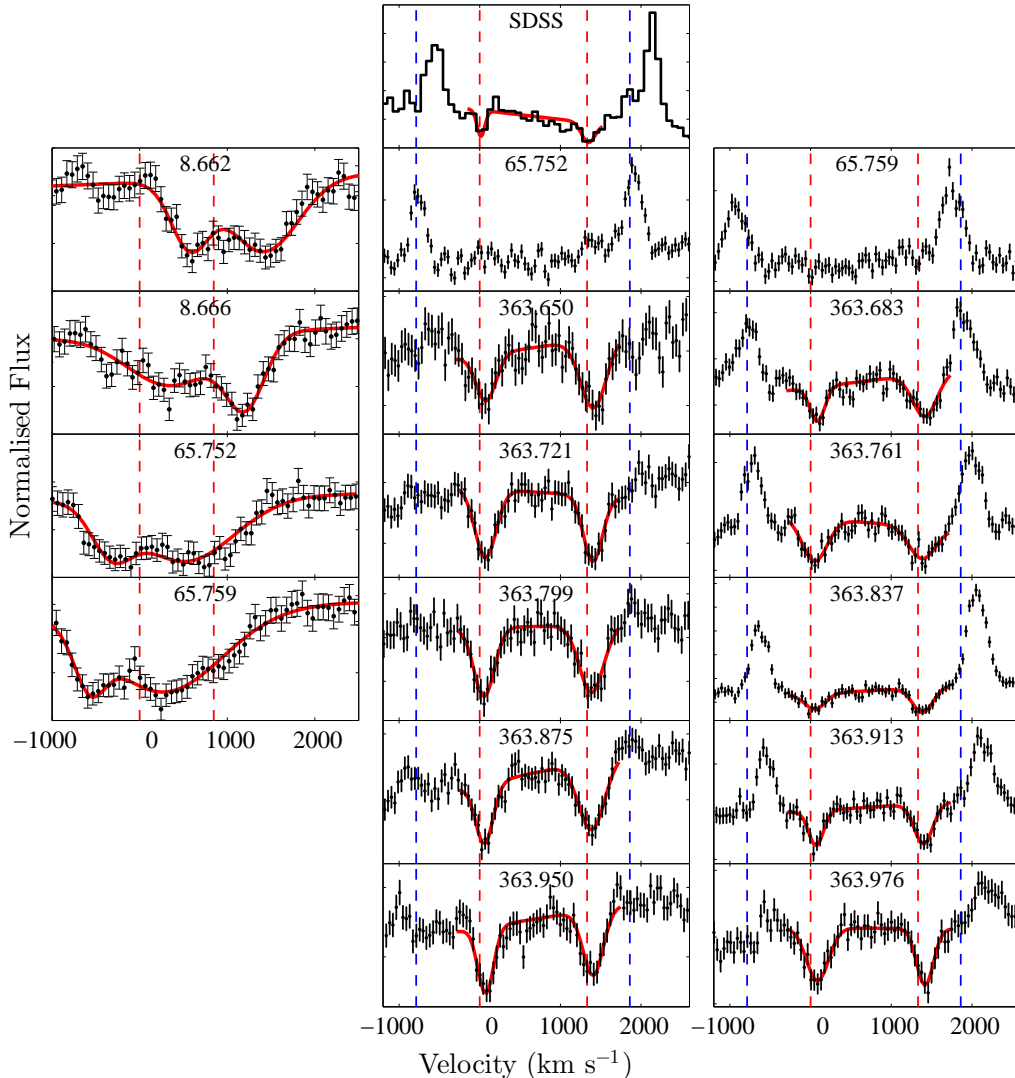


Figure 1. Left column: the region of the spectra around the Na I $\lambda\lambda 8183.26, 8194.81$ absorption doublet for observations in which it was detected. Centre and right columns: the region of the spectra around the Al I $\lambda\lambda 3944.01, 3961.52$ doublet, with the 2004 SDSS observation in the top-most panel. In all cases, the solid red curves show our best fits to the features, and the red vertical dashed lines mark the zero-velocity positions of the doublets, and the relative heliocentric Julian date (HJD-2456000) is given in the top of each panel. The regions around the aluminum doublet also contain the Ca II $\lambda\lambda 3933.66, 3968.47$ lines, which are sometimes seen in emission; the blue vertical dashed lines mark the expected zero-velocity positions of those calcium features.

and find a systemic velocity for the Ca II triplet that is very similar to that of H_β (with $\gamma = 30 \pm 7 \text{ km s}^{-1}$), and a slightly higher radial velocity amplitude ($K = 275 \pm 15 \text{ km s}^{-1}$).

3. ALUMINUM ABSORPTION DOUBLET

The Al I $\lambda\lambda 3944.01, 3961.52$ doublet is present in the spectra from 2013 March. We fit this doublet with a double-Gaussian function of a fixed separation plus a parabola to measure the radial velocity and error of the Al I doublet (Rebassa-Mansergas et al. 2007; see the middle and right panels in Figure 1). The results of this fitting are presented in Table 2. We also attempted to fit

the radial velocity curve of this Al I doublet with a sine function fixed to the binary period of 1.932 hr, but the results were unacceptable (with the χ^2 roughly 10 times higher than that for the free-period fit). The best-fitting parameters for an unconstrained period are listed in Table 3, and the radial velocity curve is shown in Figure 2. The total duration over which the relevant spectra were taken (on 2012 March 3) was only ≈ 8 hr, so we do not at all claim that this fitted period is definitive, or even that we have found evidence of any periodicity in the Al I

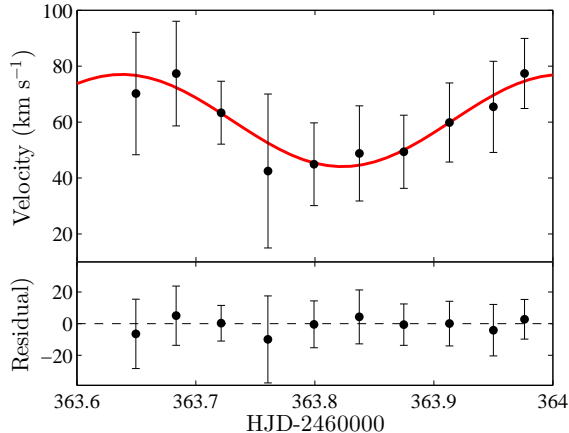


Figure 2. *Top:* the radial velocity of AlI doublet; the red curve shows our best fit to the data. *Bottom:* the residuals from our fit.

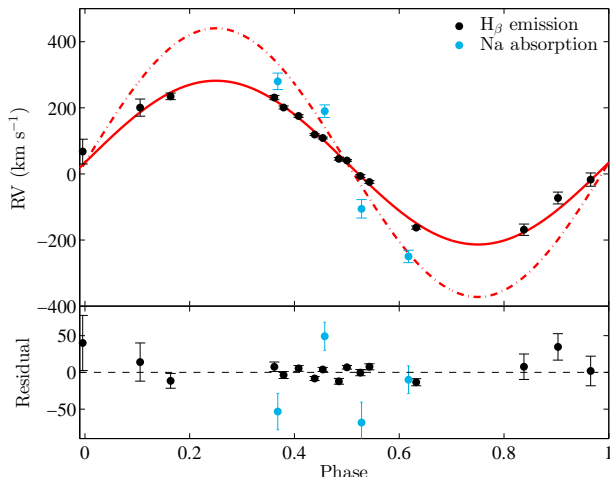


Figure 3. *Top:* the radial velocities for the $H\beta$ and NaI lines versus the orbital phase, alongside our best-fit radial velocity curves (solid and dashed-dotted curves). *Bottom:* the residuals to our best-fitting models.

doublet velocities.³

The best-fit systemic velocity (γ) for the AlI doublet is clearly inconsistent with the systemic velocity for the $H\beta$ emission lines. By itself, this is not necessarily a strong constraint on the location of the absorbing material within the system, since γ -velocities for polars are known to suffer from complications which are not seen in the population of non-magnetic CVs (van Paradijs et al. 1996). Nonetheless, this result is consistent with our later conclusion that the absorbing material is probably circumstellar.

We are confident that this AlI doublet is unlikely of telluric origin or an artifact of the telescope system, nor is it from the foreground interstellar medium, since the dispersion is about 300 km s^{-1} . Moreover, we suggest it is not from the MD, since the radial velocity amplitude and period are inconsistent with those of the NaI

absorption line from the MD (see the following section).

That AlI $\lambda\lambda 3944.01, 3961.52$ doublet is not detected in the spectra from 2012 May. Unfortunately, there is no coverage of this region in our spectra on HJD 2456008. So any inference of qualitative time variability – disappearance and reappearance – rests on upper limits derived for only two spectra from HJD 2456065 (see Figure 1 and Table 2); one of those shows very weak hints of a doublet by eye, but our fitting indicates an upper limit that is well below the later detections. The simplest interpretation is that the column density of aluminum in absorption changed between our 2012 and 2013 observations.

An alternative option to consider is that during the time of the 2012 May observations we are just not seeing the aluminum absorption. However, these spectra were taken at orbital phases of 0.54 and 0.63, and the spectrum taken at HJD of 363.683 was at an orbital phase of 0.53, which suggests that the disappearance of the aluminum absorption is not a simple function of orbital phase. The 10 spectra from HJD 363 are spread across all of the orbit, and the Al absorption lines are clearly detected in all of them.

We also find that these AlI absorption lines were detected in an SDSS spectrum of AR UMa from 2004 February (Julian day 2453061.4). If our observations are robust then any model for these lines needs to explain the disappearance of aluminum features over less than 8.2 years, and their reappearance in less than a year, with no obvious dependence on orbital phase.

We have not detected other metal absorption lines from our spectra. However, if they are present, some might perhaps have been disguised by the emission lines from the MD (e.g., MgI and CaII). Here we re-examine the far-ultraviolet spectra in Gänsicke et al. 2001, and fit the strongest metal absorption line of SiII with a Gaussian function plus a line. The result shows that the FWHM is $240 \pm 80 \text{ km s}^{-1}$, which is similar to that of the aluminum absorption doublet.

4. STELLAR PARAMETERS

AR UMa was in a low brightness state during our observations, since the molecular band from the MD was obviously presented and the continuum flux was similar to that during the low brightness state observed by Schmidt et al. (1996). It was also probably in a low accretion state, since the HeII emission line was detected in only one observation, and only with a signal-to-noise ratio below 3, which suggests that the accretion rate is minimal (Szkody et al. 1999). In the low state, the emission lines are thought to originate from the inner hemisphere of the MD, rather than the directed stream flow (Schmidt et al. 1999).

These low-state observations enable us to trace the radial velocity of the MD, and further constrain the mass of the WD with the mass and the radial velocity amplitude of the MD.

4.1. Mass of the WD

The emission lines of AR UMa originate from the hemisphere of the MD facing the WD, so their velocities' amplitudes should be smaller than that of the MD barycenter (Schmidt et al. 1999). In AR UMa, the photospheric

³ However, we note that Kalomeni (2012) found evidence for a ≈ 7.9 hour period in AR UMa by examining light variations over 11 years. This is broadly similar to that of our best fit to the radial velocity variation in the AlI doublet, although we stress that our data so far are insufficient to claim detection of a true periodicity.

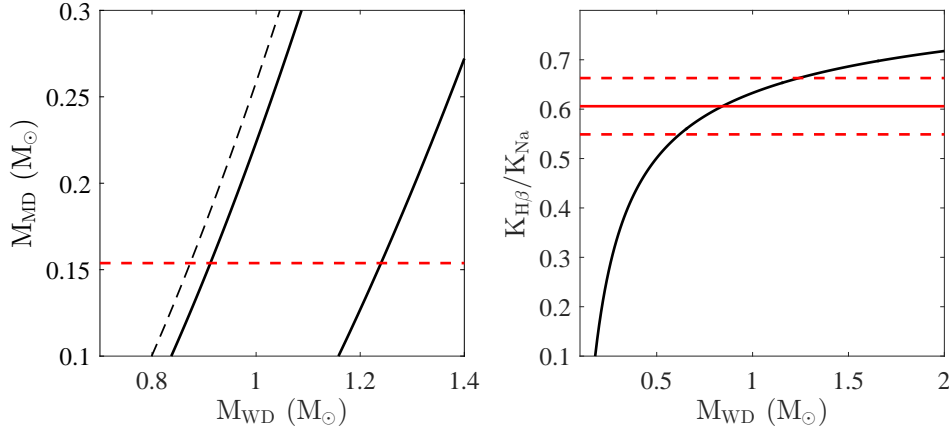


Figure 4. Left panel: the mass of the MD as a function of that of the WD. A given inclination angle fixes the mass ratio; the curves from left to right give the resulting loci in this plane for different inclination angles of 75° , 71° , and 57° . The dashed horizontal line indicates the mass of the MD as found from the semi-empirical relation for CVs (Knigge et al. 2011). Right panel: the inferred mass of the MD as a function of the amplitude ratio. The black solid curve represents the expected ratio between the radial velocity amplitudes from the L1 point and the barycenter of the MD ($K_{\text{L1}}/K_{\text{MD}}$). The ratio between the inferred $\text{H}\beta$ and NaI radial velocity amplitudes is indicated by the red solid horizontal line (with the dashed red lines showing uncertainty ranges conservatively including 3σ uncertainty in both radial velocity amplitudes).

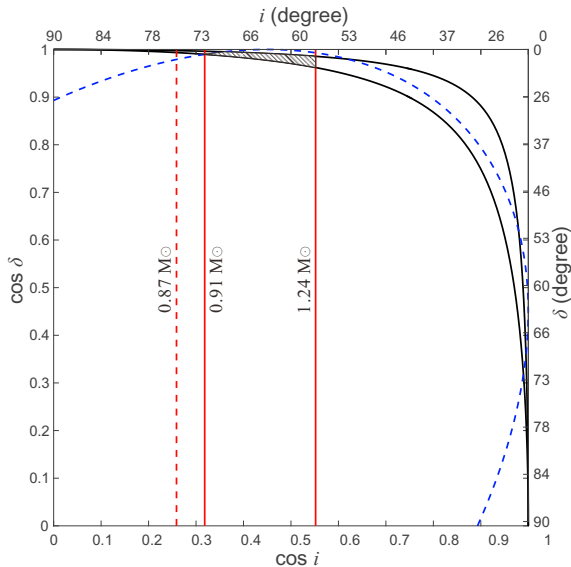


Figure 5. Constraints on the geometry of AR UMa. Only the small shaded region is allowed when combining multiple published constraints. The dashed red vertical line marks $i = 75^\circ$, and the solid red vertical lines mark $i = 71^\circ$ and 57° . The black solid and blue dashed curves represent constraints inferred from the polarization data, as described in Schmidt et al. 1999.

Na I $\lambda\lambda 8183.26, 8194.81$ doublet is more isotropically distributed over the MD (Rebassa-Mansergas et al. 2007; Schwöpe et al. 2011). This is detected in spectra from the red channel in four of the 2012 observations. We fit the doublet with a double-Gaussian function of a fixed separation plus a parabola to measure the radial velocity and error (the left panel in Figure 1). We then fit the velocity curve of Na I with a sine function, keeping γ and P fixed to the values derived from the radial velocity of $\text{H}\beta$ and the updated orbital ephemeris. The radial velocity amplitude derived from the best fitting is $K = 409 \pm 26 \text{ km s}^{-1}$ (Figure 3), i.e., higher than for the $\text{H}\beta$ lines, as expected.

We thereby estimate the mass of the MD to $0.154 M_{\odot}$ from the semi-empirical relation for CVs (see Knigge et al. 2011). This semi-empirical relation is typically taken to have an expected uncertainty below 2% (Knigge et al. 2011), although the extreme nature of AR UMa might plausibly make this estimate less reliable than for normal, non-magnetic CVs.

Since no eclipse is seen from AR UMa, the inclination angle i should be smaller than 75° (Schmidt et al. 1999), which constrains the mass of the WD to $M_{\text{WD}} > 0.87 M_{\odot}$. Harrison & Campbell (2015) found a best-fit inclination for AR UMa of 65° , which would correspond to a WD mass of $1.01^{+0.16}_{-0.14} M_{\odot}$. The uncertainty adopted here is calculated from the 90% uncertainty of the Na I amplitude. This should not be treated as giving real upper and lower limits, since no uncertainty is included for the model-fit inclination angle.

Since we expect that the barycenter of the irradiated $\text{H}\beta$ emission area should be located between the inner Lagrange point (L1) of the binary and the barycenter of the MD, this may help to constrain the mass of the WD. We first compute the ratio of the radial velocity amplitudes for the L1 point and the MD barycenter (i.e., $K_{\text{L1}}/K_{\text{MD}}$) as a function of the mass of the WD (assuming the MD mass found above), as plotted in the right panel of Figure 4. Our fits to the observed radial velocity data lead to an amplitude ratio ($K_{\text{H}\beta}/K_{\text{Na}}$) of 0.606 ± 0.057 , where the quoted uncertainty range conservatively adopts 3σ uncertainties in both the radial velocity amplitudes. The upper end of that range of statistical uncertainty corresponds to an upper limit on the WD mass of $M_{\text{WD}} < 1.24 M_{\odot}$, corresponding to an inclination angle of 57° .

This excludes a possible source of systematic uncertainty, since the Na I $\lambda\lambda 8183.26, 8194.81$ doublet may trace the outer hemisphere of the MD, i.e., be biased toward the side away from the L1 point. Nonetheless we still feel that this is probably a fairly conservative limit, as it assumes that the $\text{H}\beta$ lines trace the L1 point.

Combining this limit with the lower limit from taking

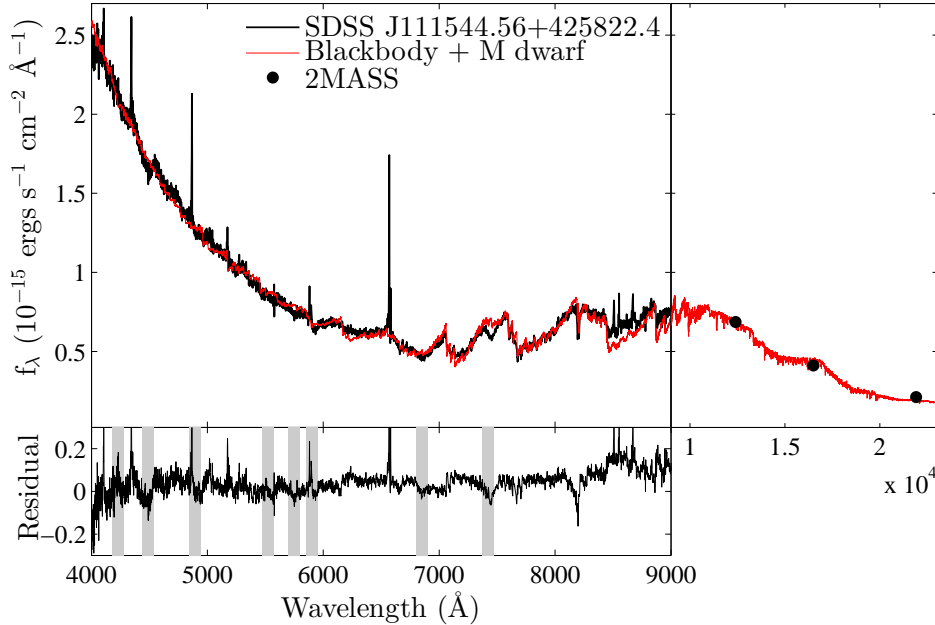


Figure 6. Top: our best-fit model spectrum (red line) compared to SDSS observations of AR UMa (black line) and 2MASS photometry (black circles). Bottom: the residual to the fits (black line). Regions in which polarization is expected to affect the spectral features are indicated by the gray shaded zones.

$i < 75^\circ$ produces an estimate for the mass range of the WD in AR UMa of $0.87 M_\odot < M_{\text{WD}} < 1.24 M_\odot$.

4.2. System Geometry

Schmidt et al. 1999 estimated the possible ranges of the inclination angle i and the colatitude of the magnetic pole δ using constraints calculated from photospheric circular polarization. Combining their results with ours ($K = 409 \pm 26 \text{ km s}^{-1}$, $0.87 M_\odot < M_{\text{WD}} < 1.24 M_\odot$), we update their constraints on i and δ to

$$57^\circ < i < 71^\circ, 10^\circ < \delta < 16^\circ, \quad (2)$$

In turn, this lower upper limit on i slightly increases the minimum inferred mass of the WD; the allowed region in Figure 5 yields a WD mass range of $0.91 M_\odot < M_{\text{WD}} < 1.24 M_\odot$.

Such system geometry ($67^\circ < i + \delta < 87^\circ$) would imply that one hotspot around the magnetic pole of AR UMa is always visible.

4.3. Spectral Decomposition

We also constructed two-component (blue and red) models based on WD and MD templates to fit our observed spectra. Since the Balmer absorption lines of the WD were undetected in the blue component of AR UMa, a series of blackbody spectra were used as WD templates. We also note that Schmidt et al. (1996) previously suggested that the blue component contained contributions from both the inner hemisphere of the MD and the atmosphere of the WD. For the MD templates, we adopt the Phoenix library of synthetic spectra (Husser et al. 2013). The model space therefore covers a WD parameter T_{bb} and MD parameters T_{eff} , $\log g$, and $[\text{Fe}/\text{H}]$. The relevant ranges in the parameter space are: WD blackbody temperature $10 \text{ kK} \leq T_{\text{bb}} \leq 50 \text{ kK}$ (step size 0.1 kK);

effective temperature $2300 \text{ K} \leq T_{\text{eff}} \leq 3400 \text{ K}$ (step size 100 K); surface gravity $0.0 \leq \log g \leq 6.0$ (every 0.5 dex); metallicity $-4.0 \leq [\text{Fe}/\text{H}] \leq 1.0$ (every 0.5 dex).

Since our spectra have limited coverage, we used the SDSS spectrum of AR UMa (SDSS J111544.56+425822.4) and minimized the χ^2 parameter to fit the spectrum in a four-dimensional parameter space, after masking all of the emission lines in the spectrum. The spectrum is reproduced at each point in the parameter space by a combination of a blackbody and a MD. They are then weighted with scaling factors that depend on the distance and the radii. The fitted spectrum (Figure 6) gives $T_{\text{bb}} = 46300 \text{ K}$, $T_{\text{eff}} = 3200 \text{ K}$, $\log g = 5.0$ and $[\text{Fe}/\text{H}] = 1.0$. The half widths of the parameters are adopted as the uncertainties (Liu et al. 2012), which are 50 K for T_{bb} and T_{eff} , 0.3 dex for $\log g$ and 0.3 dex for $[\text{Fe}/\text{H}]$.

The inferred temperature and gravity of the MD are consistent with those calculated from the semi-empirical relations of CVs ($T_{\text{eff}} \simeq 3180 \text{ K}$ and $\log g \simeq 5.1$).

However, the fitted blackbody temperature is much higher than previously estimated for the WD in AR UMa; for example, Gänsicke et al. 2001, estimated a WD temperature of $20,000 \pm 5000$ when including information from ultraviolet HST spectra of AR UMa.

The scaling factors enable us to obtain the radius of the MD and the effective radius of this blackbody component (assuming a spherical emission surface). To do this we adopt the distance of AR UMa, $86 (+10, -8) \text{ pc}$, measured from its parallax (Thorstensen et al. 2008). The derived radii are $0.15 \pm 0.02 R_\odot$ for the MD, and $0.0034 \pm 0.0004 R_\odot$ for the blue component. The radius of a non-magnetic WD with $1.01 M_\odot$ is in the range of $0.0074 < R_{\text{WD}} < 0.0084 R_\odot$, taking effective temperatures between 10000 K and 40000 K from non-magnetic DA

WD models (Holberg & Bergeron 2006; Tremblay et al. 2011)⁴. Assuming a strong internal magnetic field for the WD in AR UMa would increase the expected radius (Suh & Mathews 2000), so the emission area of the fitted blue component is too small to cover the complete surface of the WD (unless the WD is substantially more massive than we have inferred).

The inferred radius of the MD is smaller than that estimated using the semi-empirical relation for CVs, $R \simeq 0.19 R_{\odot}$. This underestimate seems consistent with the red component of the continuum being dominated by the outer hemisphere of the MD.

In Figure 6, the residuals from the fitting show features that clearly deviate from the synthetic model. Some of these are due to the polarizing effect of the strong magnetic field (Schmidt et al. 1996; Ferrario et al. 2003). The deviation around 8200Å is due to the variability of the Na I line profile (Figure 1), and the continuum around Ca II triplet may be due to the unresolved Paschen emission lines.

5. DISCUSSION

We have detected an aluminum absorption feature in spectra of AR UMa, during the probable low brightness and accretion states. The apparent sub-year time variability of the feature is especially intriguing. Here we discuss potential origins of the aluminum absorption.

5.1. Interpreting the Al I doublet as from circumstellar material

Since the radial velocity of the Al I doublet is inconsistent with that of the MD, the aluminum is unlikely to be located on the surface of the MD. Gänsicke et al. 2001 detected a P Cygni profile for Ly α emission, suggesting the existence of a moderately fast wind, about -700 km s^{-1} , from the MD, which is also inconsistent with the velocity of the Al I doublet.

Another argument against the aluminum being located on the donor star is the sub-year timescale over which we see the feature changing, given that the variation does not seem to be due to orbital changes (see Section 3). This is not a natural timescale for variations in the composition of the MD atmosphere.

The $\lesssim 8$ year timescale for disappearance of the aluminum feature could be easily explained by gravitational settling in the atmosphere of the WD. The reappearance of the aluminum in less than a year might also be naturally explained by pollution of the WD. Recent years have seen great interest in studying WDs with atmospheric heavy elements, especially because these heavy elements may have been delivered by the accretion of rocky material from a disrupted planet, debris disk, or asteroids (Zuckerman et al. 2007, 2011; Dufour et al. 2010, 2012; Pyrzas et al. 2012). Previous observations have indicated time variation in such accretion onto some isolated WDs, perhaps due to a transient gaseous disk (Wilson et al. 2014) or precession of the debris disk (Manser et al. 2015).

An alternative explanation for the presence of atmospheric heavy elements in suitably hot WDs is radiative levitation (see, e.g., Chayer et al. 1995). If the observed

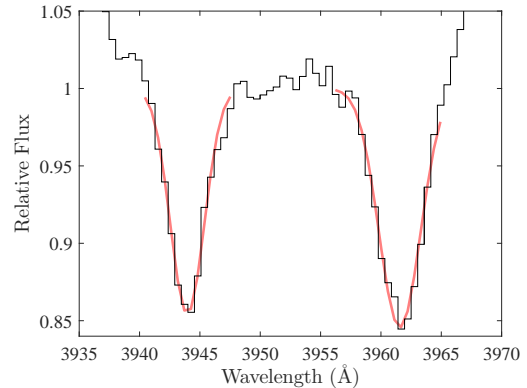


Figure 7. The fit (red line) of Al I doublet for the center-corrected combined spectrum (black line) with VPFIT.

variability had been due to the changing effect of radiative levitation on the WD, this might have suggested that the effect was rather sensitively balanced on the WD in AR UMa.

However, the profile of the Al I doublet strongly argues against the absorption feature being from the surface of the highly magnetic WD in AR UMa. All the spectral features from the atmosphere of the WD should be split into wide ranges of wavelength and be barely recognizable (Kepler et al. 2013) for AR UMa. Assuming a dipole magnetic field with a strength of ~ 240 MG at the poles gives a field strength of ~ 80 – 120 MG at the equator (Martin & Wickramasinghe 1984; Gänsicke et al. 2001). We consider it highly unlikely that a sufficiently large patch of the WD surface would have low enough magnetic field strength for the Al I doublet to be so clearly seen with no Zeeman splitting. We also note that our attempts to fit the Al I absorption line with a radial velocity curve did not produce anything consistent with that expected for the WD. Overall, we consider the lack of magnetic distortion in the lines from the Al I doublet to be convincing evidence that the lines are not formed on the surface of the WD.

Given the above, the two remaining possibilities are interstellar or circumstellar absorption. Based on the observed variability, we suggest that the absorption is unlikely to be interstellar. So we conclude that the absorption features probably have a circumstellar origin.

Gänsicke et al. (2001) found weak low-ionization lines in their FUV spectrum of AR UMa, which they interpreted as likely being due to the absorption of the local interstellar medium. Perhaps the Al I absorption doublet is from similar material as provided the origin for those low-ionization lines, in which case Gänsicke et al. (2001) also detected such circumstellar gas.

5.2. A rocky origin for the circumstellar material?

Assuming we have detected circumstellar gas in AR UMa, we now discuss the likely origin of that material. Circumstellar gas around WDs has previously been reported in four systems: WD 1040+492, WD 1942+499, WD 2257+073 and WD 1124–293 (Lallement et al. 2011; Debes et al. 2012a). An anti-correlation is derived between the effective temperature of the WD and the orbital velocity of the gas around the WDs, which is consistent with the orbiting gas material originating from the

⁴ <http://www.astro.umontreal.ca/~bergeron/CoolingModels/>

evaporation of planets or asteroids.

Additional evidence for such a scenario follows from several transit events of planets discovered from the light curve of WD 1145+017 (Vanderburg et al. 2015). The varying transit depths and their asymmetric profiles indicate a planet with a comet-like tail from evaporation. The tail, consisting of various heavy elements, would escape into the orbit through a Parker-type thermal wind (Rappaport et al. 2014; Sanchis-Ojeda et al. 2015). In that case the tail also contaminates the atmosphere of WD 1145+017.

Besides isolated WD systems, three polars – HU Aquarii, UZ Fornacis, and CSS081231:071126+440405 – are reported as having circumbinary planets (Potter et al. 2011; Qian et al. 2011; Schwöpe et al. 2015), potentially in stable highly non-coplanar orbits (Goździewski et al. 2015).

If the inferred circumstellar gas in AR UMa did originate from the evaporation of a rocky body, measuring the mass-loss flux might help to constrain the characteristics of the body evaporation (see especially Rappaport et al. 2012; Perez-Becker & Chiang 2013).

We can estimate the column density of Al I in 2013 May 12 by taking the center-corrected spectra from those observations and fitting the doublet with VPFIT (Figure 7, Carswell & Webb 2014). The best-fitting column density is $N(\text{Al I}) = 3.9 \pm 0.2 \times 10^{13} \text{ cm}^{-2}$. Unfortunately, the spacing of our observations does not sufficiently constrain the timescale of evaporation to provide a useful estimate of the mass-loss flux.

We estimate that the region in which an aluminum-rich rock would be expected to sublimate is much larger than the volume in which Zeeman splitting would have been detected in our low-resolution spectra (corresponding to a field strength of roughly 2 MG, and a distance from the WD of $\approx 0.05 R_{\odot}$). Taking a sublimation temperature for Corundum (Al_2O_3) of 1500 K, we find that the equilibrium temperature caused by heating from the WD would exceed this value within $\approx 1.6 R_{\odot}$ from the WD. This is very similar to the major axis of the orbit of the MD. Moreover, this is comparable to the separation at which the WD would tidally disrupt such an asteroid (assuming a density of 4.02 g cm^{-3} for Corundum); for asteroids with lower density, tidal disruption would likely begin before evaporation (see, e.g., Veras et al. 2014).

We note that the relative radial velocity of the fitted Al I doublet to the AR UMa binary system is $\approx 27 \text{ km s}^{-1}$, which is consistent with circumstellar gas detected around other WDs (Lallement et al. 2011).

We do not claim that it is inevitable that this interpretation of circumstellar aluminum demands a rocky origin. An alternative possibility might be related to a proposed explanation for the known CVs with suprasolar photospheric abundances of aluminum (Sion et al. 2001; Gänsicke et al. 2005; José et al. 2006). Some models for those CVs indicate that aluminum was likely generated in nova outbursts on the WD, and furthermore that the aluminum-enriched nova ejecta might have been captured by the donor star and re-accreted onto the WD (Marks & Sarna 1998; Sengupta et al. 2013; Sion & Sparks 2014). If our interpretation that the aluminum in AR UMa is circumstellar is correct, then it might perhaps be explained by a variation of that model,

if some of the nova ejecta can remain within the system. However, it is less obvious to us how the time variation we observe might be naturally explained in this model.

So a tentative potential explanation for the origin of this circumstellar gas is that AR UMa possesses an extrasolar analog to the Oort cloud (Stone et al. 2015) or the Kuiper Belt (Bonsor et al. 2011) containing some Al-rich rocks. The orbits of those rocks might become destabilized due to perturbation of the binary motion or dynamical interaction with other planets in the system (Debes et al. 2012b; Frewen & Hansen 2014), after which they approach so close to the WD as to be evaporated, resulting in circumstellar gas in the form of a highly eccentric ring (Veras et al. 2014, 2015) or spherical cloud around the WD (Stone et al. 2015). That circumstellar gas may accrete on to the WD with a time-scale of less than ~ 8.2 years due to the additional force from the MD (Veras et al. 2014), which might explain the time-scale over which the aluminum absorption disappears.

If this scenario is correct, more time-resolved spectra of these lines may provide a way to probe the duty cycle of the evaporation and further shed light on the population of asteroids in AR UMa and their orbital instabilities. Additional infrared spectroscopy might constrain the composition of the gas by detecting molecular features and thus investigate the character of these asteroids (Carry 2012).

6. SUMMARY

We have detected an aluminum absorption doublet in spectra of AR UMa, and suggest that this is evidence for circumstellar material in this extreme polar. The aluminum absorption feature also appears to be time-variable, having disappeared over less than 9 years, and then re-appeared in less than a year. Our spectra also allowed a preliminary attempt to better-constrain the properties of the components in AR UMa, including an updated estimate for the WD mass in the range of $0.91 M_{\odot} < M_{\text{WD}} < 1.24 M_{\odot}$.

A potential explanation for this variable aluminum absorption is irregular circumstellar gas due to evaporation of rocky material from, e.g., asteroids destabilized from orbits further out in the system. We encourage studies of AR UMa with high time-resolution spectra, both to enable deeper investigation of the origin of this absorption and to help further improve our understanding of this extreme system.

We sincerely thank Patrick Dufour for valuable discussions, especially for important clarifications regarding the Zeeman effect in the very strong field regime. We are also grateful to an anonymous referee for forcing us to re-examine our initial interpretation, and to Koji Mukai, Jay Farihi, and Rosanne Di Stefano for very helpful thoughts. This research uses data obtained through the Telescope Access Program (TAP), which is funded by the National Astronomical Observatories and the Special Fund for Astronomy from the Ministry of Finance. This work was supported by the Chinese National Natural Science Foundation (NSFC) through grants NSFC-11333004/11425313, and the National Astronomical Observatories, Chinese Academy of Sciences under the Young Researcher Grant. S.J. thanks

the Chinese Academy of Science for support through the President's International Fellowship Initiative grant No. 2011Y2JB07.

REFERENCES

- Beust, H., Vidal-Madjar, A., Ferlet, R., & Lagrange-Henri, A. M. 1990, *A&A*, 236, 202
- Beust, H., Lagrange, A.-M., Plazy, F., & Mouillet, D. 1996, *A&A*, 310, 181
- Bonsor, A., Mustill, A. J., & Wyatt, M. C. 2011, *MNRAS*, 414, 930
- Carry, B. 2012, *Planet. Space Sci.*, 73, 98
- Carswell, R. F., & Webb, J. K. 2014, *Astrophysics Source Code Library*, ascl:1408.015
- Chayer, P., Vennes, S., Pradhan, A. K., et al. 1995, *ApJ*, 454, 429
- Debes, J. H., Kilic, M., Faedi, F., et al. 2012a, *ApJ*, 754, 59
- Debes, J. H., Walsh, K. J., & Stark, C. 2012b, *ApJ*, 747, 148
- Dickinson, N. J., Barstow, M. A., Welsh, B. Y., et al. 2012, *MNRAS*, 423, 1397
- Dufour, P., Kilic, M., Fontaine, G., et al. 2010, *ApJ*, 719, 803
- Dufour, P., Kilic, M., Fontaine, G., et al. 2012, *ApJ*, 749, 6
- Ferrario, L., Wickramasinghe, D. T., & Schmidt, G. 2003, *MNRAS*, 338, 340
- Frewen, S. F. N., & Hansen, B. M. S. 2014, *MNRAS*, 439, 2442
- Gänsicke, B. T., Schmidt, G. D., Jordan, S., & Szkody, P. 2001, *ApJ*, 555, 380
- Gänsicke, B. T., Szkody, P., Howell, S. B., & Sion, E. M. 2005, *ApJ*, 629, 451
- Goździewski, K., Słowikowska, A., Dimitrov, D., et al. 2015, *MNRAS*, 448, 1118
- Harrison, T. E., & Campbell, R. K. 2015, *ApJS*, 219, 32
- Holberg, J. B., & Bergeron, P. 2006, *AJ*, 132, 1221
- Holman, M. J., & Wiegert, P. A. 1999, *AJ*, 117, 621
- Howell, S. B., Gelino, D. M., & Harrison, T. E. 2001, *AJ*, 121, 482
- Husser, T.-O., Wende-von Berg, S., Dreizler, S., et al. 2013, *A&A*, 553, A46
- José, J., Hernanz, M., & Iliadis, C. 2006, *Nuclear Physics A*, 777, 550
- Kalomeni, B. 2012, *MNRAS*, 422, 1601
- Karmann, C., Beust, H., & Klinger, J. 2003, *A&A*, 409, 347
- Kepler, S. O., Pelisoli, I., Jordan, S., et al. 2013, *MNRAS*, 429, 2934
- Knigge, C., Baraffe, I., & Patterson, J. 2011, *ApJS*, 194, 28
- Lallement, R., Welsh, B. Y., Barstow, M. A., & Casewell, S. L. 2011, *A&A*, 533, A140
- Liu, C., Li, L., Zhang, F., et al. 2012, *MNRAS*, 424, 1841
- Manser, C. J., Gänsicke, B. T., Marsh, T. R., et al. 2015, *arXiv:1511.02230*
- Marks, P. B., & Sarna, M. J. 1998, *MNRAS*, 301, 699
- Martin, B., & Wickramasinghe, D. T. 1984, *MNRAS*, 206, 407
- Perez-Becker, D., & Chiang, E. 2013, *MNRAS*, 433, 2294
- Potter, S. B., Romero-Colmenero, E., Ramsay, G., et al. 2011, *MNRAS*, 416, 2202
- Pyrzas, S., Gänsicke, B. T., Brady, S., et al. 2012, *MNRAS*, 419, 817
- Qian, S.-B., Liu, L., Liao, W.-P., et al. 2011, *MNRAS*, 414, L16
- Rappaport, S., Levine, A., Chiang, E., et al. 2012, *ApJ*, 752, 1
- Rappaport, S., Barclay, T., DeVore, J., et al. 2014, *ApJ*, 784, 40
- Rebassa-Mansergas, A., Gänsicke, B. T., Rodríguez-Gil, P., Schreiber, M. R., & Koester, D. 2007, *MNRAS*, 382, 1377
- Remillard, R. A., Schachter, J. F., Silber, A. D., & Slane, P. 1994, *ApJ*, 426, 288
- Sanchis-Ojeda, R., Rappaport, S., Pallè, E., et al. 2015, *ApJ*, 812, 112
- Schmidt, G. D., Szkody, P., Smith, P. S., et al. 1996, *ApJ*, 473, 483
- Schmidt, G. D., Hoard, D. W., Szkody, P., et al. 1999, *ApJ*, 525, 407
- Schwöpe, A. D., Horne, K., Steeghs, D., & Still, M. 2011, *A&A*, 531, A34
- Schwöpe, A. D., Mackebrandt, F., Thinius, B. D., et al. 2015, *Astronomische Nachrichten*, 336, 115
- Sengupta, S., Izzard, R. G., & Lau, H. H. B. 2013, *A&A*, 559, A66
- Sion, E. M., Cheng, F.-H., Szkody, P., et al. 2001, *ApJ*, 561, L127
- Sion, E. M., & Sparks, W. 2014, *ApJ*, 796, L10
- Stone, N., Metzger, B. D., & Loeb, A. 2015, *MNRAS*, 448, 188
- Suh, I.-S., & Mathews, G. J. 2000, *ApJ*, 530, 949
- Szkody, P., Vennes, S., Schmidt, G. D., et al. 1999, *ApJ*, 520, 841
- Thorstensen, J. R., Lépine, S., & Shara, M. 2008, *AJ*, 136, 2107
- Tremblay, P.-E., Bergeron, P., & Gianninas, A. 2011, *ApJ*, 730, 128
- Vanderburg, A., Johnson, J. A., Rappaport, S., et al. 2015, *Nature*, 526, 546
- van Lieshout, R., Min, M., & Dominik, C. 2014, *A&A*, 572, A76
- van Paradijs, J., Augusteijn, T., & Stehle, R. 1996, *A&A*, 312, 93
- Veras, D., Leinhardt, Z. M., Bonsor, A., Gänsicke, B. T. 2014, *MNRAS*, 445, 2244
- Veras, D., Leinhardt, Z. M., Eggl, S., Gänsicke, B. T. 2015, *MNRAS*, 451, 3453
- Wilson, D. J., Gänsicke, B. T., Koester, D., et al. 2014, *MNRAS*, 445, 1878
- Zuckerman, B., Koester, D., Melis, C., Hansen, B. M., & Jura, M. 2007, *ApJ*, 671, 872
- Zuckerman, B., Koester, D., Dufour, P., et al. 2011, *ApJ*, 739, 101

APPENDIX

We present the fits of the H_{β} emission lines in our data (see Fig. 8), and of the first line ($\lambda = 8498 \text{ \AA}$) in the Ca II triplet (see Fig. 9). For a radial-velocity fit to the Ca II triplet in Fig. 9, we keep P fixed to the value from the updated orbital ephemeris.

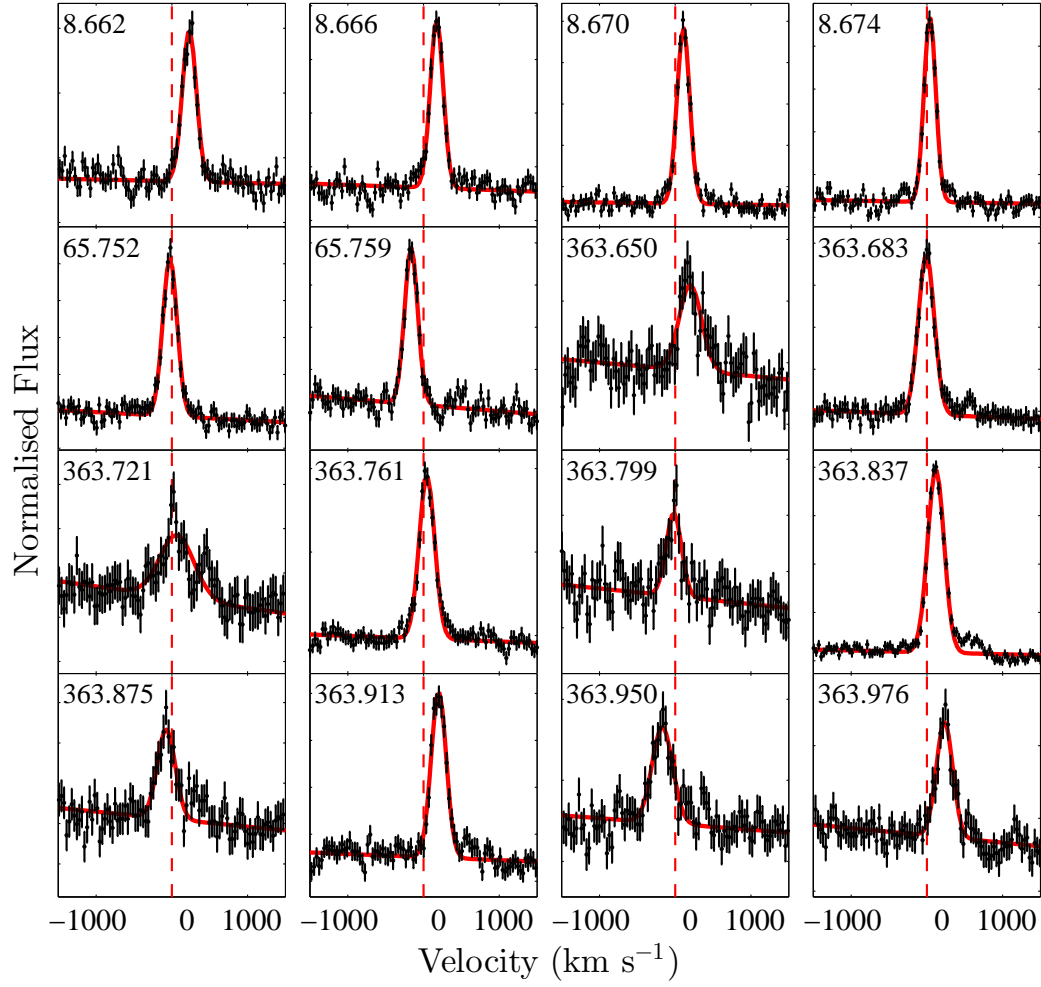


Figure 8. Region of the spectra around the H β emission line. The best fits are shown as red solid lines, and the red vertical dashed lines mark the zero-velocity positions. The heliocentric Julian date-2456000 is given in the top left corner of each panel.

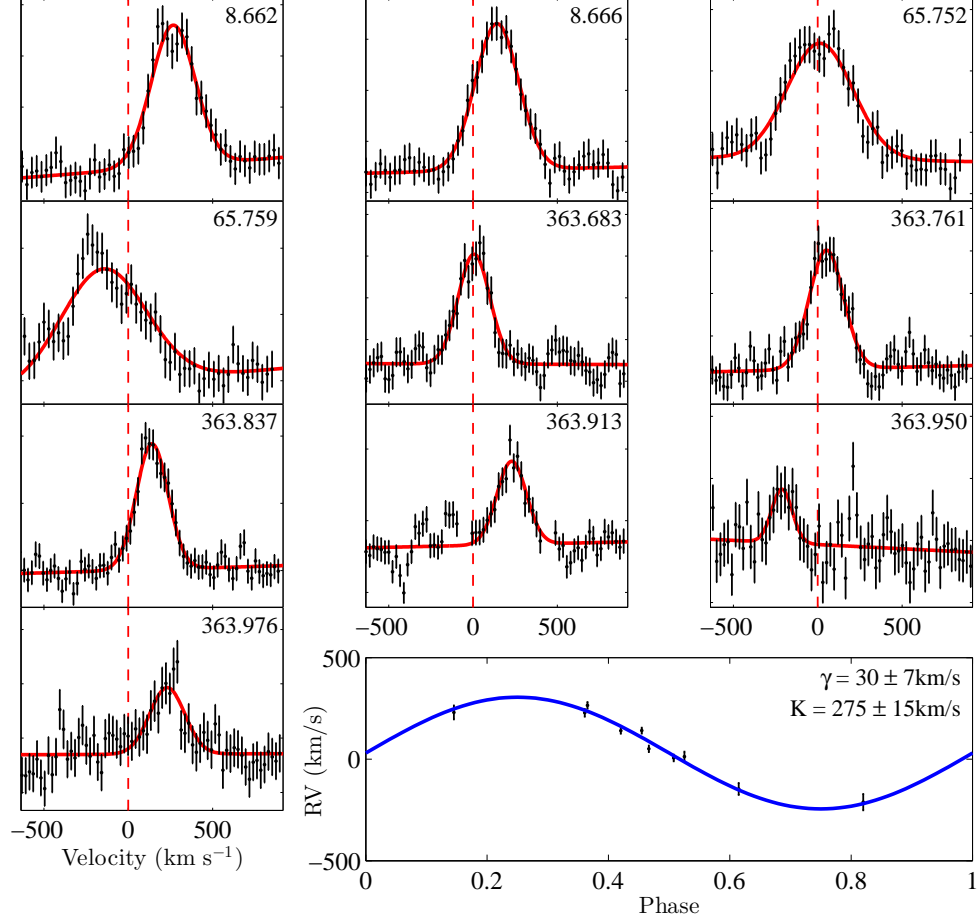


Figure 9. Region of the spectra around $\lambda = 8498 \text{ \AA}$. The best fits are shown as red solid lines for the first line of the CaII triplet, and the red vertical dashed lines mark the zero-velocity positions. The heliocentric Julian dates-2456000 are given in the top right corners of the first 10 panels. Our best-fitting radial velocity (RV) curve is shown as the blue solid line in the bottom right panel. The fitted systemic velocity (γ) and the radial velocity amplitude (K) are presented in the top right corner of the panel.